Available online at www.sciencedirect.com

ScienceDirect

Geochimica et Cosmochimica Acta 132 (2014) 375–390

Geochimica et Cosmochimica Acta

www.elsevier.com/locate/gca

In situ Raman study and thermodynamic model of aqueous carbonate speciation in equilibrium with aragonite under subduction zone conditions

Sébastien Facq [a], Isabelle Daniel [a,*], Gilles Montagnac [a], Hervé Cardon [a], Dimitri A. Sverjensky [b,c]

[a] *Laboratoire de Géologie de Lyon: Terre, Planètes, Environnement, Université Claude Bernard Lyon1, ENS de Lyon, CNRS, UMR 5276, 2 rue Raphaël Dubois, 69622 Villeurbanne, France*

[b] *Dept. Earth & Planetary Sciences, Johns Hopkins University, 3400 N. Charles St., Baltimore, MD 21218, USA*

[c] *Geophysical Laboratory, Carnegie Institution of Washington, 5251 Broad Branch Road NW, Washington, DC 20015, USA*

Received 31 May 2013; accepted in revised form 22 January 2014; available online 4 February 2014

Abstract

Carbonate minerals may be recycled into the mantle at subduction zones. However, the evolution of carbonate minerals in equilibrium with aqueous fluids as well as the nature of the chemical species of dissolved carbon in the deep crust and mantle at high *PT* conditions are still unknown. In this study, we report an integrated experimental and theoretical study of the equilibration of $CaCO_3$ minerals with pure water at subduction zone conditions over the pressure and temperature ranges 5–80 kbar and 300–400 °C. The fluid speciation was studied using *in situ* Raman spectroscopy. The relative amounts of dissolved carbonate and bicarbonate were estimated from the corrected areas of the Raman bands of the carbonate and bicarbonate ions and used to constrain a theoretical thermodynamic model of the fluid speciation and solubility of aragonite. At 300–400 °C, our results indicate that the proportion of dissolved C present as CO_2 strongly decreases in fluids in equilibrium with aragonite at $P > 10$ kbar. CO_2 is replaced by HCO_3^- and $CaHCO_3^+$ which predominate until $P > 40$ kbar, where CO_3^{2-} and $CaCO_3^0$ become the dominant C-species. At higher temperatures, the theoretical model indicates that CO_2 again becomes a major species in fluids in equilibrium with aragonite depending on the pressure.
© 2014 Elsevier Ltd. All rights reserved.

1. INTRODUCTION

Over geological time scales, the carbon cycle is driven by the exchange of carbon between Earth's interior and exosphere that strongly impacts levels of atmospheric carbon dioxide over millions of years (Berner, 1999). Subduction zones link geologically surficial and deep Earth carbon reservoirs and modulate the carbon cycle. Many studies have therefore focused on geochemical fluxes of carbon at subduction zones (Evans, 2012 and references therein). The total input of carbon at present-day subduction rates is estimated to $5.4–8.8 \times 10^{13}$ g of C year^{-1} (Dasgupta, 2013). Comparison of the pressure–temperature paths of subduction slabs worldwide with available experimental boundaries of decarbonation and melting of subducted lithologies (Dasgupta, 2013) suggest that most of this carbon input may return to the deep mantle with minor degassing only through arc volcanism (e.g., Yaxley and Green, 1994; Kerrick and Connolly, 1998, 2001; Dasgupta et al., 2005; Thomsen and Schmidt, 2008; Dasgupta and Hirschmann, 2010; Tsuno and Dasgupta, 2012; Dasgupta, 2013). However, the arc flux

* Corresponding author.
E-mail address: Isabelle.Daniel@univ-lyon1.fr (I. Daniel).

http://dx.doi.org/10.1016/j.gca.2014.01.030
0016-7037/© 2014 Elsevier Ltd. All rights reserved.

of CO_2 requires significant recycling up to 70% by arc magmatism (Sano and Williams, 1996).

This puzzle might be solved if carbon were released in the mantle and ultimately to the exosphere through arc volcanism by the dissolution of carbonate minerals driven by the release of fluids from the subducted slab (Frezzotti et al., 2011). In that case, knowledge of the solubility of carbonate minerals, especially the most abundant one in sediments ($CaCO_3$), and the speciation of aqueous carbon under subduction zone conditions is critical to modeling of the carbon cycle.

The solubility of $CaCO_3$ minerals and the aqueous speciation of C have been investigated in great detail at ambient conditions and temperatures up to 90 °C (Plummer and Busenberg, 1982; Morse and MacKenzie, 1990). Some studies are available at higher temperatures and pressures (Walther and Long, 1986; Fein and Walther, 1989; Newton and Manning, 2002; Caciagli and Manning, 2003; Stefansson et al., 2013), extending as high as 800 °C and 17 kbars. The larger ranges of pressures and temperatures relevant to subduction zones in the upper mantle remain essentially unexplored experimentally (Martinez et al., 2004; Sanchez-Valle, 2013) and theoretically (Dolejš and Manning, 2010; Dolejš, 2013), leaving great uncertainty as to the dominant forms of aqueous C-species in equilibrium with carbonate minerals, particularly at pressures greater than about 20 kbar.

In the present study, we combine experimental and theoretical approaches to investigate the equilibrium of carbonate minerals with water in a new regime of pressures and temperatures. The fluid speciation was studied using *in situ* Raman spectroscopy coupled to a Diamond Anvil Cell (DAC) from 5 to 80 kbar at 300–400 °C (Fig. 1). The latter conditions overlap with those estimated along the surface of some cold subducting slabs (Syracuse et al., 2010) as indicated in Fig. 1. The Raman data are used to constrain a theoretical thermodynamic model of the fluid speciation in equilibrium with aragonite in order to quantify the equilibrium constants corresponding to carbonate mineral solubility and aqueous carbon speciation. Recent advances in theoretical aqueous geochemistry enable the application and testing of aqueous species equations of state at much higher pressures than previously possible (Sverjensky et al., 2013; Manning et al., 2013; Pan et al., 2013). Using the experimental results of the present study to constrain these equations of state is a first step towards the development of quantitative theoretical models of carbon transport by aqueous fluids in subduction zones.

2. EXPERIMENTAL AND THEORETICAL APPROACHES

2.1. Experimental methods

The aqueous speciation experiments were carried out in a membrane-type Diamond Anvil Cell (DAC) (Chervin et al., 1995) equipped with synthetic IIa diamond anvils with culet diameters of 500 μm. An aqueous fluid and a crystal of calcite were loaded in a pre-indented 100 μm thick rhenium gasket, drilled with a 200-μm-diameter hole. The

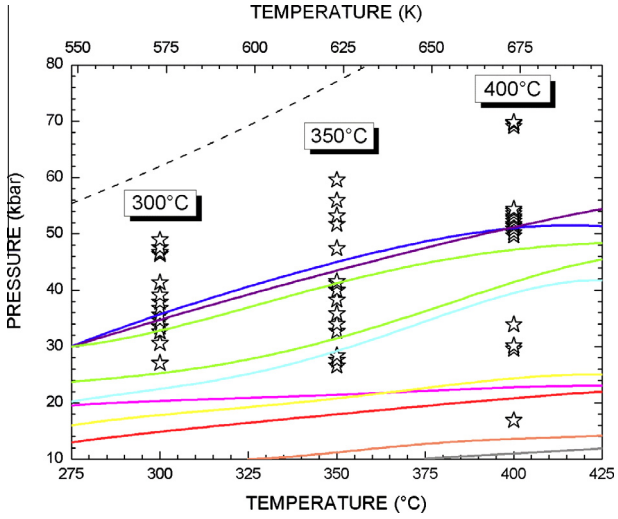

Fig. 1. Stars represent the *PT* conditions investigated in the present study. Raman spectra were collected along isotherms (300, 350 and 400 °C respectively) with increasing pressure. Dashed curve locates the melting curve of H_2O (Datchi et al., 2000). Colored curves represent *PT* paths of the slab surface for some worldwide arc segments according the W1300 model of Syracuse et al., 2010 (same colors as in Fig. 1, Syracuse et al., 2010). (For interpretation of the references to color in this figure legend, the reader is referred to the web version of this article.)

aqueous fluid consists of double-distilled and deionized water (18 MΩ cm) with neutral pH. The initial concentration of $CO_{2,aq}$ is therefore negligible. The crystal of calcite was cut from the same natural single crystal used by Caciagli and Manning (2003) from Rodeo (Durango, Mexico). The DAC was first externally heated by a surrounding resistive coil until the temperature of the sample reached the targeted temperature (300, 350 or 400 °C). The temperature of the sample was measured with a K-type thermocouple glued on a diamond anvil as close as possible to the culet. The pressure inside the compression chamber was then increased using an automatic pressure regulator (Sanchez technologies™). Pressure was calculated from the *PT* calibrated shift of the carbonate v_1 symmetric stretching mode of a crystal of aragonite (Fig. 2A and B). This calibration method has been singled out over traditional high *PT* calibrations using either ruby or $SrB_4O_7:Sm^{2+}$ as a pressure sensor to avoid any chemical contamination of the fluid. As the v_1 symmetric stretching mode of aragonite is quasi-harmonic (Gillet et al., 1993), the frequency evolution of this vibrational mode as functions of pressure and temperature may be considered separately:

$$v_1(P) = v_1(T_0, P_0) + b * P \quad (1)$$

$$v_1(T) = v_1(T_0, P_0) + a_1 * T + a_2 * T^2 \quad (2)$$

The parameters a_1, a_2, b and $v_1(T_0, P_0)$ were obtained from the fits on our experimental data (Fig. 2) and the pressure P inside the compression chamber could be calculated as a function of temperature T by combining Eqs. (1) and (2):

$$P = \frac{v_1(P) - v_1(T_0, P_0) - a_1 * T - a_2 * T^2}{b} \quad (3)$$

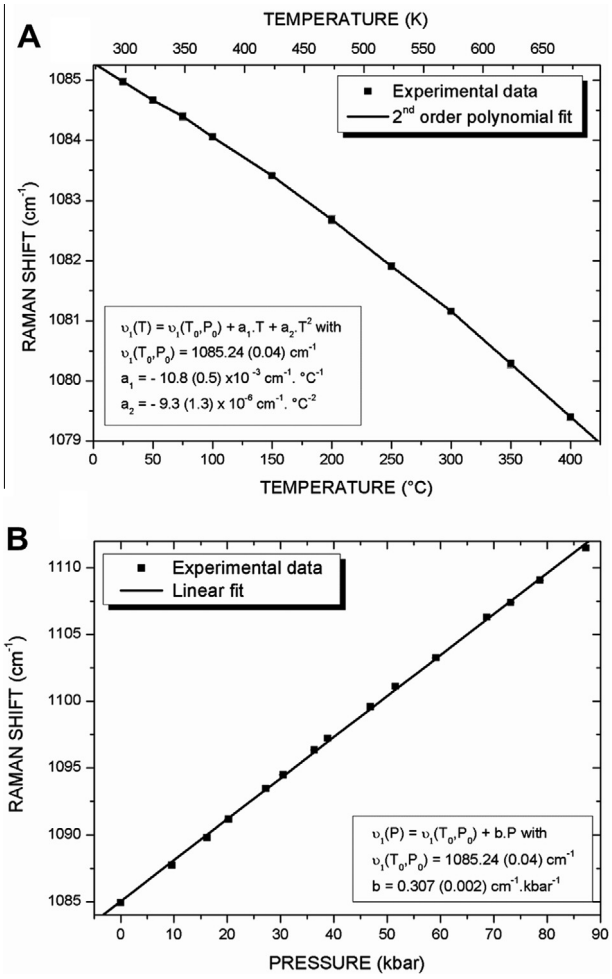

Fig. 2. Frequency evolution of the carbonate ν_1 symmetric stretching mode of aragonite as a function of temperature (A) and pressure (B).

Raman spectra were collected in the 800–1300 cm^{-1} spectral region using a confocal Labram HR800 Raman spectrometer (Horiba Jobin–Yvon™) of 800 mm focal length. A spectral resolution of 0.3 cm^{-1} was reached with a holographic grating of 1800 $gr.mm^{-1}$ and a Peltier-cooled front illuminated CCD detector (1024 × 256 pixels). The grating was kept in a fixed position, in order to achieve an accuracy of 0.1 cm^{-1} or better, which was mandatory for calculating pressure from the ν_1 shift in the carbonate crystal. The excitation line at 514.5 nm was produced by an Ar^+ laser source (Spectra Physics™) focused on the sample using a Mitutoyo™ 50× long working distance objective (0.42 N.A.). The laser power at the sample was 10 mW.

Raman spectra were collected along isotherms (Fig. 1) in the 800–1300 cm^{-1} spectral range and then analyzed. A linear baseline was subtracted and then the peak features were determined using a commercial least-squares fitting procedure (Peakfit™) assuming Voigt profiles for the Raman bands.

2.2. Theoretical methods

A theoretical model of aqueous speciation in equilibrium with aragonite was constructed as a complement to the experimental data collected. Because the Raman data were collected in a novel region of *PT* space, they serve in part as a test of the applicability of theoretical aqueous geochemical calculations under such conditions. Considerable support for this approach comes from the implementation of density model extrapolations into the elevated pressure and temperature regime (Dolejš and Manning, 2010; Dolejš, 2013; Manning et al., 2013) where comparisons with experimentally measured solubilities can be made.

In the present study, equilibrium constants involving aqueous species were calculated using the revised Helgeson–Kirkham–Flowers (HKF) equations of state (Shock and Helgeson, 1988, 1990; Shock et al., 1989, 1997; Sverjensky et al., 1997) for the standard partial molal Gibbs free energies of the individual species. Additional revisions to the equation of state parameters for some of the species were made to take account of more recent thermodynamic data (see below). Values of the dielectric constant of water needed for the HKF equation of state for the standard Gibbs free energies were obtained from an equation of state linking the experimental data of Heger et al. (1980) with predictions made using the theoretical equation applied by Franck et al. (1990). The latter were extrapolated using correlations with the density of water (Sverjensky et al., 2013) and tested with *ab initio* molecular dynamics calculations (Pan et al., 2013). The density of water was computed with the equations of Zhang and Duan (2005), applicable from 1 to about 60 kbar.

Aqueous ion activity coefficients were calculated assuming that the extended Debye–Hückel equation (Helgeson et al., 1981) could be empirically extrapolated from 5.0 kbar to high pressure using the density of water. Aqueous activity coefficients of neutral species were assumed to be unity. In the calcium carbonate–water system, this approach was successfully used to model calcite solubility to 30 kbar (Manning et al., 2013). At the ionic strengths encountered in the calculations, the activity coefficients of the ions did not contribute significantly to the overall uncertainties in the theoretical model. It is typical of many aqueous geochemical calculations (with the exception of brines) that more substantial uncertainties typically arise from the standard free energies of the species in the system (Helgeson et al., 1981). All the speciation solubility calculations were carried out with the computer code EQ3 (Wolery, 1983) and a custom-built data file.

The thermodynamic properties of calcite were taken from Berman and co-workers (Berman, 1988; Berman and Aranovich, 1996). The properties of aragonite were derived by fitting the Berman heat capacity equation as a function of temperature to calculated values based on a model of vibrational data (Matas et al., 2000) and by fitting the Berman volume equation to experimental data extending to 800 °C and 82 kbar (Martinez et al., 1996). The standard Gibbs free energy of formation of aragonite at 25 °C and 1 bar was calculated from the experimental solubility

product (Plummer and Busenberg, 1982). The entropy of aragonite was derived from consistency with published experimentally reversed phase equilibria between calcite and aragonite.

3. RESULTS

3.1. Equilibration of a $CaCO_3$ crystal with water at 400°C

Fig. 3 illustrates the evolution of a fragment of a natural single crystal of calcite at equilibrium with pure water inside the compression chamber during compression at 400 °C and Fig. 4 shows the corresponding Raman spectra measured in the aqueous fluid. At 16.9 kbar, the Raman spectrum contains a single Raman band at 997.8 cm^{-1} assigned to the v_5 C—OH symmetric stretching mode of the bicarbonate ion (Frantz, 1998). At this moderate pressure, calcite is soluble enough that bicarbonate can be detected (detection limit of 5.10^{-3} m). Carbonate had a similar detection limit but is only present at very low concentrations at these lower pressures. It becomes detectable at pressures in excess of 30 kbar. Detection limits were established for these species based on known aqueous solutions of sodium carbonate and bicarbonate in the same apparatus used for the experimental studies.

According to the C_S (σ_h) symmetry, the bicarbonate ion has eight other Raman active modes, the v_7 (OH), v_6 (CO) and v_4 (COH) bending modes at 632, 672, and 1302 cm^{-1}, respectively, the v_8 (CO_3) out-of-plane deformation mode at 841 cm^{-1} and overtone at 1684 cm^{-1}, the v_3 (CO) symmetric and v_2 (CO) asymmetric stretching modes at 1360 and 1630 cm^{-1}, respectively and the v_1 (OH) stretching mode at 2650 cm^{-1} (Davis and Oliver, 1972). None of the weak Raman bands mentioned above could not be detected in such a dilute system.

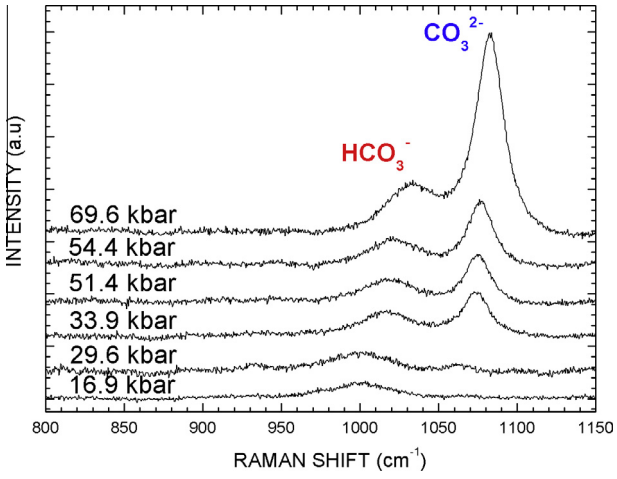

Fig. 4. Evolution of the Raman spectra in the aqueous fluid in the 800–1300 cm^{-1} spectral range as a function of pressure during dissolution of the $CaCO_3$ crystal at 400 °C.

At 29.6 kbar, the calcite–aragonite phase transition is observed by changes in both the optical aspect and the Raman spectrum of the crystal. The crystal of calcite initially loaded (Fig. 3A) has completely dissolved in the aqueous

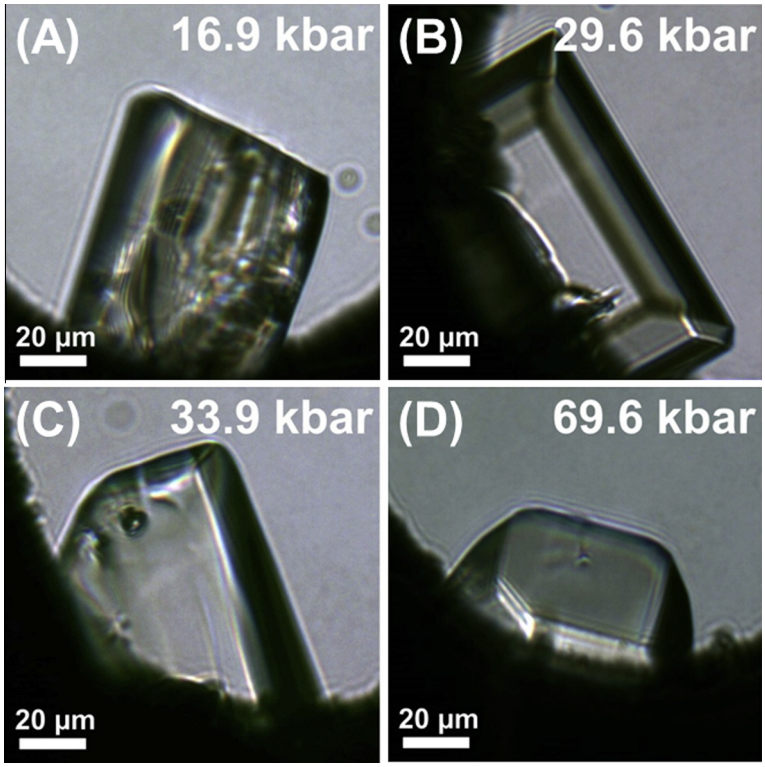

Fig. 3. Evolution at 400 °C as a function of pressure of a single crystal of calcite observed by microscopy inside the compression chamber. During dissolution of the $CaCO_3$ crystal, the phase transition calcite – aragonite is observed at 29.6 kbar (pictures A and B).

fluid and a new crystal of aragonite (Fig. 3B) has nucleated and grown elsewhere in the compression chamber. At the same time, the v_1 symmetric stretching mode of carbonate ions of the $CaCO_3$ crystal is red-shifted by about $7.42 \pm 0.02\ cm^{-1}$. This value agrees well with the difference of $8.30 \pm 0.48\ cm^{-1}$ between the frequencies of the carbonate v_1 mode of aragonite and calcite, respectively, calculated for the same PT conditions using the present independent temperature and pressure calibration of aragonite (Fig. 2) and calcite I (not shown here). It is also in good agreement with the value of $6.11 \pm 1.24\ cm^{-1}$ calculated from Gillet et al. (1993).

Aragonite and calcite I were the two carbonate minerals optically observed or identified by Raman spectroscopy. The high-pressure metastable calcite-II and calcite-III obtained at 14 and 19 kbar, respectively, during compression of calcite at ambient temperature (Fong and Nicol, 1971; Gillet et al., 1988; Liu and Mernagh, 1990; Fiquet et al., 1994; Suito et al., 2001) did not form in the course of the present experiments because of the high temperature conditions. Moreover, the temperature was low enough to avoid the orientational order/disorder phase transition observed in calcite at low pressure (Mirwald, 1976, 1979; Dove and Powell, 1989; Redfern et al., 1989) or even the aragonite–disordered calcite phase transition observed above 20 kbar (Suito et al., 2001).

The Raman spectrum measured in the aqueous fluid at 29.6 kbar (see Fig. 4) exhibits an additional weak Raman band located at $1061.8\ cm^{-1}$ assigned to the v_1 symmetric stretching mode of dissolved carbonate ions (Oliver and Davis, 1973). According to the D_{3h} symmetry of the carbonate ion, five other Raman active modes are expected, the v_4 in plane deformation mode at $684\ cm^{-1}$, the v_2 out-of-plane deformation mode at $880\ cm^{-1}$ and overtone at $1761\ cm^{-1}$ and the v_3 at 1380 (1436) cm^{-1} (Davis and Oliver, 1972). None of these weak bands were observed in our Raman spectra in the present relatively dilute system.

Upon further compression, the new crystal of aragonite progressively dissolves in the aqueous fluid leading to a decrease in its volume of 63% between 29.6 and 69.6 kbar, as calculated from the changes in size and shape of the crystal inside the compression chamber. The crystal also takes on a rounded shape, characteristic of dissolution (Fig. 3C and D). These changes resulted in a gradual increase of the intensity of the v_1 mode of dissolved carbonate ions and v_5 mode of dissolved bicarbonate ions due to the progressive release of these two C-species in the aqueous fluid during compression. Similar behavior was observed during dissolution experiments conducted at 300 and 350 °C.

3.2. Distribution of the dissolved C-species

The relative amounts of dissolved carbonate and bicarbonate have been estimated as a function of pressure from the area of the Raman bands of the carbonate and bicarbonate ions v_1 and v_5 symmetric stretching modes, respectively for the temperatures 300, 350 and 400 °C, after correction from their relative Raman cross-sections and temperature dependence (Frantz, 1998). Fig. 5 presents the evolution of the relative amounts of dissolved carbonate and bicarbonate in equilibrium with $CaCO_3$ at 300, 350 and 400 °C as a function of pressure. The solid curves are best fits to our experimental data using an empirical sigmoidal function:

$$y = 100/[1 + \exp(A * (X - B))] \quad (4)$$

In Eq. (4), A and B are constants whose values are given in Table 1. The pressures of the calcite–aragonite phase transition predicted at thermodynamic equilibrium (according to Lin and Huang, 2004) and those experimentally observed are represented by arrows and dotted lines, respectively. The transition is observed at pressures greater than equilibrium values, probably due to the metastable persistence of calcite at the relatively low temperatures of our experiments. It shifts progressively towards equilibrium pressures as temperature increases. At 350 °C, the phase transition was promoted by the addition of a small fragment of a natural crystal of aragonite and occurs closer to the equilibrium pressure. Aragonite is present in all our experiments at pressures higher than 30 kbar, which is the regime of greatest interest in the present study.

Fig. 5 shows that bicarbonate (HCO_3^-) is the predominant dissolved C-species detected spectroscopically in the aqueous fluid for pressures less than about 30 kbar at 300–400 °C. Carbonate becomes the predominant C-species above about 40 kbar. Over the entire pressure range investigated from 1 bar to 70 kbar, the data clearly show a progressive change in the proportions of bicarbonate to carbonate. They become equal at about 40 kbar. This pressure, called here the pressure of equimolality, is temperature dependent and exhibits a slight linear increase with temperature from 38.4 ± 0.4 kbar at 300 °C to 39.9 ± 0.6 kbar at 400 °C (Table 1). This can be explained by the slight increase in solubility with temperature as already reported for calcite (Caciagli and Manning, 2003).

The overall behavior of carbonate and bicarbonate can be seen in Fig. 6, which shows the evolution of the pressure of equimolality and the pressures for which the relative amounts of carbonate or bicarbonate are greater than 80% as a function of temperature. The pressure domains where carbonate or bicarbonate are dominant dissolved C-species in the fluid are represented by the upper and lower hatched zones, respectively. This figure shows that carbonate is by far the major aqueous C-species at high pressure at these temperatures.

4. DISCUSSION AND THEORETICAL MODEL

4.1. Speciation derived from Raman spectroscopy

The speciation of carbon dissolved in aqueous fluids at elevated pressures and temperatures is critical to understanding the solubility of $CaCO_3$ minerals and the mass transport of carbon in the mantle. One previous set of experimental studies focused on calcite solubilities at temperatures up to 600 °C, but at the relatively low pressures of 1–3 kbar using an extraction–quench hydrothermal apparatus (Walther and Long, 1986; Fein and Walther, 1987, 1989). The solubility data were interpreted assuming that the dominant dissolved species were Ca^{2+}, $CO_{2,aq}$

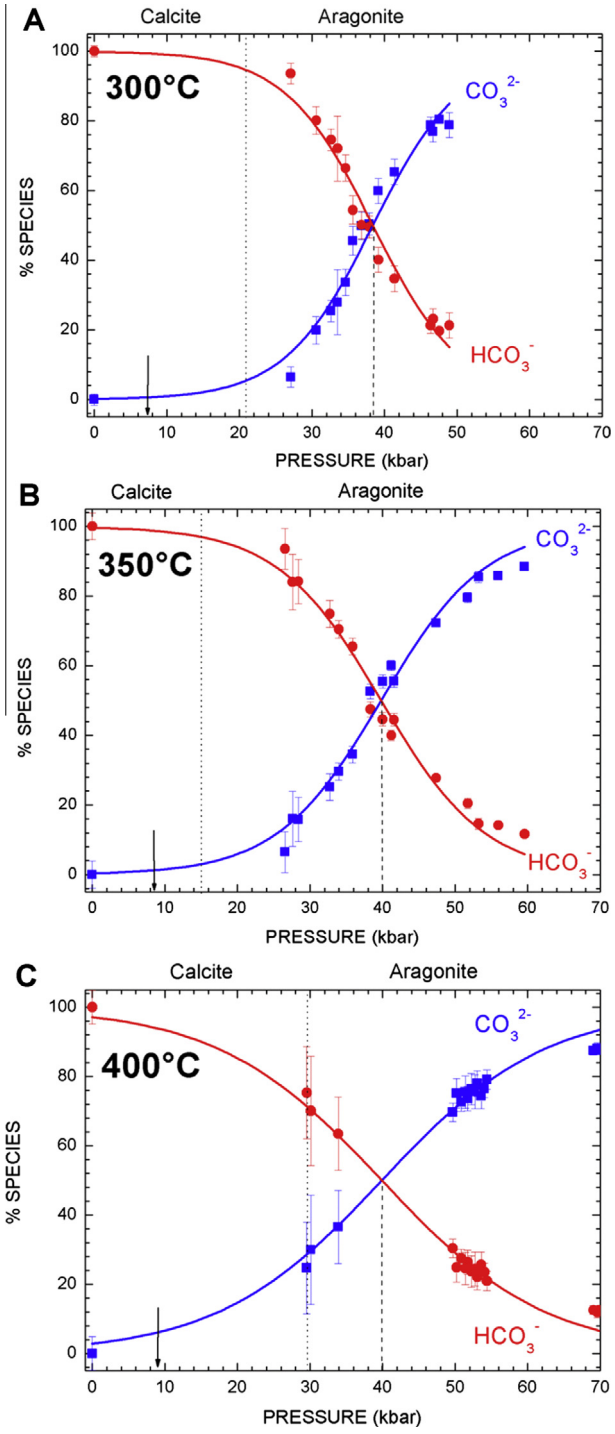

Fig. 5. Pressure dependence of the relative amounts of dissolved carbonate (blue) and bicarbonate (red) in equilibrium with a $CaCO_3$ crystal at 300 (A), 350 (B) and 400 °C (C). (For interpretation of the references to color in this figure legend, the reader is referred to the web version of this article.)

and HCO_3^- (Fein and Walther, 1987, 1989). No evidence was found of the formation of aqueous complexes between the aqueous HCO_3^- and CO_3^{2-} and sodium or calcium in solutions with log $m_{Na} < -1.0$ at 2 kbar and 400–600 °C (Fein and Walther, 1989).

More recently, the temperature and pressure fields of these studies were extended to 800 °C and 16 kbar using a piston–cylinder apparatus (Newton and Manning, 2002; Caciagli and Manning, 2003). From these solubility measurements and by extrapolation of thermodynamic data for HCO_3^-, Caciagli and Manning (2003) inferred that $CO_{2,aq}$ was the dominant C-species under their experimental conditions whereas CO_3^{2-}, $CaHCO_3^+$ and $CaCO_{3,aq}$ were negligible ($\ll$1%) in the experimental fluids.

In the course of the present experiments, the Raman spectra never showed any signal consistent with the presence of dissolved carbon dioxide (i.e. $CO_{2,aq}$). Neither the Fermi peak located at 1285 cm^{-1} (Colthup et al., 1975) nor the "hot band" generally present at high pressure and high temperatures conditions below 1285 cm^{-1} (Dubessy et al., 1999) were observed, probably because they were below the detection limit in the present study. The detection limit for $CO_{2,aq}$ is as high as 200 mmolal with the present experimental design, which required a fixed grating to calculate pressure from the ν_1 mode of the carbonate crystal. The CO_2 Fermi peak at 1285 cm^{-1} is very close to the C—C mode of the diamond anvil (1332 cm^{-1} at ambient conditions) and becomes invisible at high pressure due to their rather contrasted compressibility and intensity (see Fig. 5B, Frantz, 1998). It appears from the *in situ* Raman data (see Fig. 4) that carbonate and bicarbonate species, which may include Ca-complexes of these species, are the major C-species present in the aqueous fluid. These observations are consistent with the composition of the fluid inclusions identified by Raman spectroscopy in ultrahigh-pressure rocks from the Italian western Alps (Frezzotti et al., 2011), which exhibit the presence of carbonate and bicarbonate ion and a lack of CO_2. Raman spectroscopy cannot currently be used to distinguish between isolated carbonate or bicarbonate ion and Ca-complexes of these ions at the relatively low total dissolved C concentrations of the present study, unlike in other systems like sulfate (e.g. Frantz et al., 1994; Schmidt, 2009).

Although our experiments represent a novel realm of pressures and temperatures not previously investigated for carbonate equilibria, our results are consistent with established trends extending from lower to higher pressures. Equilibrium constants calculated with the HKF equations of state for the aqueous species in SUPCRT92 (Johnson et al., 1992) can be used only for $P \leqslant 5$ kbar, but they clearly show that the progressive ionization of $CO_{2,aq}$ to HCO_3^- and to CO_3^{2-} is favored by increasing pressure and decreasing temperature, consistent with the results of decades of study of aqueous dissociation reactions (Helgeson and Kirkham, 1976; Sverjensky et al., 1997). Compared to previous studies of carbonate mineral solubility, our study refers to extremely high pressures and relatively low temperatures. Under these conditions it can be expected that $CO_{2,aq}$ would tend to be ionized to HCO_3^- and CO_3^{2-}. Overall, the distinctive differences between our Raman speciation results at 30 to 70 kbar and the previous interpretations of calcite solubilities at pressures up to about 20 kbar emphasize the necessity of experimental measurements over a wide range of pressures and temperatures relevant to the upper mantle.

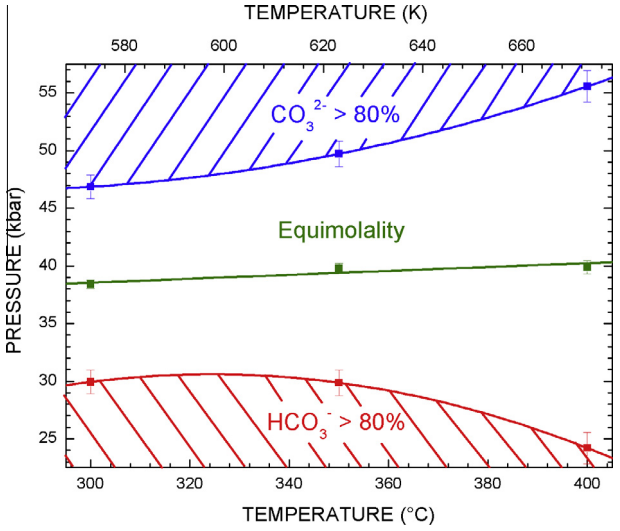

Fig. 6. Evolution of the pressure of equimolality between carbonate and bicarbonate species (green curve) and of the pressures for which the relative amount of carbonate and bicarbonate are superior to 80% (blue and red curves respectively). (For interpretation of the references to color in this figure legend, the reader is referred to the web version of this article.)

4.2. Theoretical thermodynamic model

4.2.1. Aqueous speciation and solubility model

Based on previous extensive low temperature studies of carbonate mineral solubility and aqueous speciation (e.g. Plummer and Busenberg, 1982; Morse and Mackenzie, 1990; Stefansson et al., 2013), a theoretical model of the aqueous speciation in equilibrium with aragonite and water in the diamond anvil cell requires simultaneous consideration of the following equilibria:

$$CaCO_3^{Arag.} = Ca^{2+} + CO_3^{2-} \quad (5)$$

$$HCO_3^- = H^+ + CO_3^{2-} \quad (6)$$

$$CO_2 + H_2O = H^+ + HCO_3^- \quad (7)$$

$$H_2O = H^+ + OH^- \quad (8)$$

$$CaHCO_3^+ = Ca^{2+} + HCO_3^- \quad (9)$$

$$CaCO_3^0 = Ca^{2+} + CO_3^{2-} \quad (10)$$

Assuming pure aragonite, the corresponding Law of Mass Action expressions are as follows:

$$K_{Arag.} = a_{Ca^{2+}} a_{CO_3^{2-}} \quad (11)$$

$$K_{HCO_3^-} = \frac{a_{H^+} a_{CO_3^{2-}}}{a_{HCO_3^-}} \quad (12)$$

$$K_{CO_2^0} = \frac{a_{H^+} a_{HCO_3^-}}{a_{CO_2^0} a_{H_2O}} \quad (13)$$

$$K_{H_2O} = a_{H^+} a_{OH^-} \quad (14)$$

$$K_{CaHCO_3^+} = \frac{a_{Ca^{2+}} a_{HCO_3^-}}{a_{CaHCO_3^+}} \quad (15)$$

$$K_{CaCO_3^0} = \frac{a_{Ca^{2+}} a_{CO_3^{2-}}}{a_{CaCO_3^0}} \quad (16)$$

The standard Gibbs free energies of formation of all the aqueous species indicated in Eqs. (5)–(10) were calculated using the HKF equations of state (Table 2). The basic form of the equations proved to be very appropriate for describing the experimental trends with temperature and pressure. However, at the extremely high pressures of the present study revisions to some of the key equation of state coefficients for some species were necessary. For example, although preliminary calculations indicated that estimates of the dissociation constant of water from Marshall and Franck (1981) are useful at high temperatures and modest pressures, extrapolation of these estimates to the relatively low temperatures and extremely high pressures of the present study led to internally inconsistent results. Consequently, equation of state coefficients used in the present study for the OH^- ion were based on an equation of state fit to the estimations given by Bandura and Lvov (2006) as described in Table 2 and the Appendix (see Fig. A1).

For the aqueous C-bearing species, revisions were based in part on the values given in Shock and Helgeson (1988) and Shock et al. (1989), but also took into account new data. For example, in the case of aqueous CO_2, the equation of state coefficients from Shock et al. (1989) were revised to take into account new high temperature experimental heat capacity and volume data (analyzed by Plyasunov and Shock, 2001) which extend to 350 °C at low pressures (Appendix Fig. A2A). At the same time, consistency was maintained with experimental data for the solubility of CO_2 gas from 0 to 350 °C (Appendix Fig. A2B). Similarly, the equation of state coefficients of the HCO_3^- ion were revised for better consistency with experimental dissociation constant data from 25 to 250 °C at $P_{sat.}$ (Appendix Fig. A2C). In this way, the temperature dependence of the thermodynamic model is supported by auxiliary data from the literature, as well as the Raman

Table 1
Parameters A and B of the Eq. (4) used to fit experimental Raman data presented in Fig. 5, pressure of equimolality between carbonate and bicarbonate species and pressures for which the relative amount of carbonate and bicarbonate greater than 80% for each temperature investigated in this study.

Temperature (°C)	A	B	$P_{HCO_3^-}$ > 80% (kbar)	$P_{equimolality}$ (kbar)	$P_{CO_3^{2-}}$ > 80%(kbar)
300	0.164 (12)	38.4 (4)	29.9 (10)	38.4 (4)	46.9 (10)
350	0.140 (9)	39.8 (4)	29.9 (11)	39.8 (4)	49.7 (11)
400	0.088 (4)	39.9 (6)	24.2 (14)	39.9 (6)	55.6 (14)

Table 2
Equation of state coefficients for use in the revised HKF equations of state for aqueous species consistent with the equilibrium constants given in Table 3. The parameters were taken from Shock and Helgeson (1988) and Shock et al. (1989) unless otherwise noted. Major revisions were made to the a_1 values for the species CO_2^0 and CO_3^{2-} (see text).

Species	ΔG_f^{0} [a]	ΔH_f^{0} [b]	S^{0} [b]	C_P^{0} [b]	V^{0} [c]	a_1 [d]	a_2 [a]	a_3 [e]	a_4 [f]	c_1 [b]	c_2 [f]	ω [a]
Ca^{2+}	−132,120	−129,800	−13.5	−7.5	−18.1	−0.25[g]	−7.25[g]	5.0[g]	−2.49	9.0	−2.5	1.24
OH^-	−37,595	−54,977	−5.0[h]	−19[h]	−9.1[h]	2.1[h]	−5.0[h]	1.0[h]	−2.7[h]	12.1[h]	−7.5[h]	1.72
CO_2^0	−92,250	−98,900	28.1	52.1	32.8	7.79[i]	3.14[i]	2.2[i]	−2.9	37.0[i]	6.5[i]	−0.2[i]
HCO_3^-	−140,282	−164,989	23.5	−8.5	24.6	7.65[j]	0.92[j]	0.60[j]	−2.82	11.0[k]	−3.8[k]	1.27
CO_3^{2-}	−126,191	−161,385	−12.95	−65.0	−5.0	5.80[m]	5.0[m]	−2.0[l]	−10.8[m]	18.0[m]	−20.0[m]	4.6[m]
$CaHCO_3^+$	−273,830[n]	−294,350	16.0[n]	91.0[n]	37.5[n]	9.14[n]	4.42[n]	1.13[n]	−2.96[n]	65.9[n]	15.5[n]	0.70[n]
$CaCO_3^0$	−262,750[o]	−287,390	0.0[o]	14.0[o]	21.5[o]	6.66[o]	2.05[o]	3.12[o]	−2.86[o]	32.8[o]	−0.2[o]	2.00[o]

[a] cal mol^{-1}.
[b] cal mol^{-1} K^{-1}.
[c] cm^{-3} mol^{-1}.
[d] cal mol^{-1} bar^{-1}.
[e] cal K mol^{-1} bar^{-1}.
[f] cal K mol^{-1}.
[g] Value of a_1, predicted from a revised correlation with ΔV_n^0 for divalent ions (Fig. 11B); a_2 calculated from a_1 and the experimental value of σ (Shock and Helgeson, 1988); a_4 predicted from a_2 and the correlation in Shock and Helgeson (1988); a_3 calculated from consistency with the experimental value of V^0 at 25 °C and 1 bar (Shock and Helgeson, 1988).
[h] Retrieved from fitting the equilibrium constant for the dissociation constant of water at $P_{sat.}$ (Sweeton et al., 1974) and at elevated pressure and temperature (Bandura and Lvov, 2006).
[i] Value of a_1, predicted from a revised correlation of a_1, with ΔV_n^0 (Sverjensky et al., 2014); a_2 calculated from a_1, and a predicted value of σ; a_4 predicted from a_2 and the correlation in Shock and Helgeson (1988); a_3 calculated from consistency with the experimental value of V^0 at 25 °C and 1 bar (Shock et al., 1989); c_1, c_2 and ω from fitting experimental heat capacities to 300 °C from Hnedkovsky and Wood (1997) and gas solubilities (see Appendix Fig. A2).
[j] Value of a_1, retrieved from fitting the equilibrium constant log $K_{HCO_3^-}$ (Table 3) as a function of pressure; a_2 calculated from a_1, and an experimental value of σ from Shock and Helgeson (1988); a_4 calculated from a_2 and the correlation in Shock and Helgeson (1988); a_3 calculated from the other parameters and the experimental value of V° (Shock and Helgeson, 1988).
[k] Value of c_1, from fitting experimental equilibrium with CO_2 at $P_{sat.}$ with the experimental Cp at 25 °C and 1 bar and the correlation of Cp and c_2 from Shock and Helgeson (1988; see Appendix Fig. A2C).
[l] Calculated from the experimental value of V^0 at 25 °C and 1 bar (Shock and Helgeson, 1988) and the remaining parameters in the volume equation of state.
[m] Retrieved from fitting the equilibrium constant log $K_{Arag.}$ (Table 3) as a function of pressure and temaperature.
[n] Values of S^0, C_p^0, V^0 and ω all retrieved from the experimental data of Plummer and Busenberg (1982) and log K values derived in the present study from fitting calcite solubility data from Caciagli and Manning (2003; Appendix Figs. A3 and A4); a_1, predicted from a revised correlation of a_1, with ΔV_n^0 (Sverjensky et al., 2014); a_2 calculated from a_1, and a predicted value of σ; a_4 predicted from a_2 and the correlation in Shock and Helgeson (1988); a_3 calculated from consistency with the experimental value of V^0 at 25 °C and 1 bar; c_1, from fitting the equilibrium constants with the C_p at 25 °C and 1 bar and the correlation of C_p and c_2 from Shock and Helgeson (1988).
[o] Values of S^0, C_p^0, V^0 and to all retrieved from the experimental data of Plummer and Busenberg (1982) and log K values derived in the present study from fitting the Raman data of the present study (Appendix Fig. A4); a_1, predicted from a revised correlation of a_1, with ΔV_n^0 (Sverjensky et al., 2014); a_2 calculated from a_1, and a predicted value of σ; a_4 predicted from a_2 and the correlation in Shock and Helgeson (1988); a_3 calculated from consistency with the experimental value of V^0 at 25 °C and 1 bar; c_1, from fitting the equilibrium constants with the C_p at 25 °C and 1 bar and the correlation of C_p and c_2 from Shock and Helgeson (1988).

speciation data of the present study, and is well calibrated from 0 to 400 °C.

It was also clear from the outset of this study that the equation of state parameters for the CO_3^{2-} ion from Shock and Helgeson (1988) were the least well-established, compared to Ca^{2+}, OH^-, CO_2 and HCO_3^-, because they were not based on experimental values of the volumes and heat capacities as functions of temperature. It therefore could be expected that the predicted properties of the CO_3^{2-} ion at elevated pressures and temperatures would be subject to much greater uncertainty than those of CO_2 and HCO_3^-. As will be shown below, this indeed turned out to be the case. The final values for the CO_3^{2-} ion adopted in the present study (Table 2) represent revised values based on the Raman speciation as discussed below.

In addition, we included the reactions in Eqs. (9) and (10) in our speciation model because preliminary solubility calculations using the revised equation of state coefficients of CO_2 and HCO_3^- indicated that the $CaHCO_3^+$ complex was useful to fit the data of Caciagli and Manning (2003) and because the temperature dependence of the equilibrium constants log $K_{Arag.}$ and log $K_{HCO_3^-}$ derived from the Raman data exhibited a sensible decrease with increasing temperature when the $CaCO_3^0$ complex was included. It should be emphasized that direct spectroscopic evidence of these species at elevated pressures is not available. However, both complexes have previously been studied in detail from 0 to 90 °C (Plummer and Busenberg, 1982) and preliminary equation of state representations of $CaHCO_3^+$ and $CaCO_3^0$ were previously given in Shock and Koretsky

(1995) and Sverjensky et al. (1997), respectively. The equation of state coefficients of these complexes were revised in the present study to preserve a consistent description of the data from Plummer and Busenberg (1982), the solubilities of calcite from Fein and Walther (1989) and Caciagli and Manning (2003), and the Raman data at pressures of 40–50 kbar as detailed below.

The equation of state representation of the $CaHCO_3^+$ complex was calibrated using equilibrium constants obtained by fitting the experimental solubilities of calcite (Caciagli and Manning, 2003) at 500–700 °C and pressures up to 17 kbar (Appendix Fig. A3). In this way, the calibration of the temperature dependence of our thermodynamic model was extended to 700 °C. It is interesting to note that although the $CaHCO_3^+$ complex is thought to be important at the conditions studied by Caciagli and Manning (2003), and is predicted to be significant in the lower parts of the pressure range of the present study (see below), it disappears at the highest pressures of the present study, where the abundance of CO_3^{2-} favors the formation of the $CaCO_3^0$ complex. Our equation of state representation of the latter complex was calibrated using some, but not all, of the Raman speciation data of the present study as described below.

Solubility and speciation calculations were carried out in order to regress the experimental Raman speciation data every 10 kbar at pressures of 30–60 kbar (Fig. 7, Table 3). It should be noted that at pressures below 30 kbar, the model curves in Fig. 7 represent extrapolative predictions based on the equations of state for the aqueous species. These indicate small but significant amounts of carbonate ion (e.g. 5–20% of the total of carbonate plus bicarbonate), but the solubilities of the aragonite are sufficiently low that these small amounts of carbonate ion were not detectable by Raman spectroscopy. In the regression calculations, predicted equilibrium constants corresponding to the reactions in Eqs. (7)–(9) were used (as indicated in Table 3), based on the revised properties of the species OH^-, CO_2 and $CaHCO_3^+$. The experimental speciation data were regressed between 30 and 60 kbar to obtain new values of $K_{\text{Arag.}}$, $K_{HCO_3^-}$, and K_{CaCO_3} (denoted by the asterisks in Table 3). Because the CO_3^{2-} ion occurs in both Eqs. (5) and (6), new values for the two equilibrium constants $K_{\text{Arag.}}$ and $K_{HCO_3^-}$ represented a single regression parameter at a given pressure and temperature. Simultaneous regression for the other equilibrium constant (K_{CaCO_3}) was included at 30–50 kbar to ensure that the temperature dependence of the values of $K_{\text{Arag.}}$ and $K_{HCO_3^-}$ between 300 and 400 °C at elevated pressures were consistent with the equation of state representation based on the known temperature dependence of $K_{HCO_3^-}$ between 0 and 250 °C at low pressures (see Fig. 10D below). At 60 kbar, equation of state predictions of K_{CaCO_3} were used. The fact that these predictions gave sensible results in the speciation model and are consistent with the low temperature and pressure experimental dissociation constant data (Appendix Fig. A4) provides strong support to the internal consistency of the aqueous speciation model over a very wide range of temperatures and pressures.

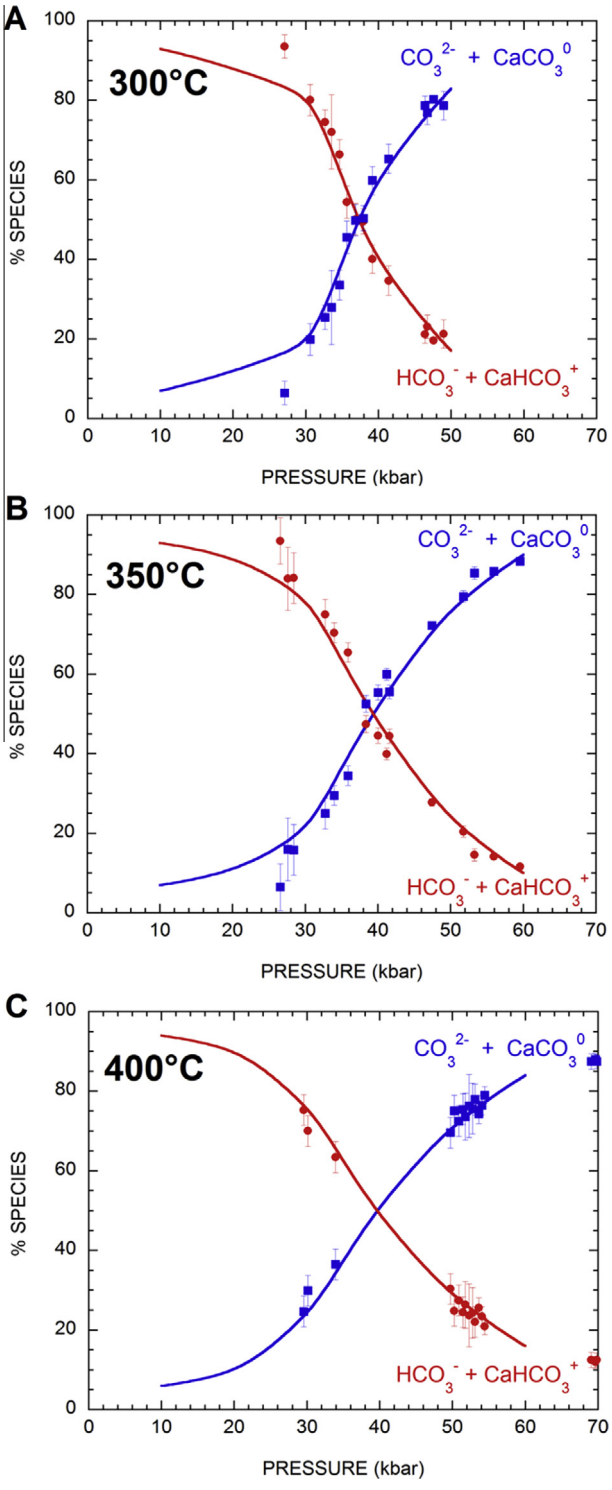

Fig. 7. Theoretically calculated curves from a speciation-solubility model of aragonite in equilibrium with aqueous solution at 300 (A), 350 (B) and 400 °C (C) under oxidizing conditions. The curves were constrained to fit the Raman speciation data by retrieving the equilibrium constants $K_{\text{Arag.}}$, $K_{HCO_3^-}$, $K_{CaHCO_3^+}$, and $K_{CaCO_3^0}$ (Table 3) using the equation of state parameters for the aqueous species given in Table 2.

Table 3
Equilibrium constants used to calculate model aqueous speciation and aragonite solubilities in fitting and extrapolating the experimentally derived proportions of HCO_3^- and CO_3^{2-} derived from the Raman spectra and calculating the solubilities in Figs. 7 and 8. Equilibrium constants obtained by regression are marked with an asterisk.

T (°C)	P (kbar)	log $K_{CaHCO_3^+}$	log $K_{CaCO_3^0}$	log K_{CO_2}	log $K_{HCO_3^-}$	log $K_{Arag.}$	log K_{OH^-}
300	10	−1.96	−3.92	−5.38	−8.30	−7.63	8.53
	20	−0.83	−2.76	−3.64	−7.10	−5.68	7.55
	30	0.09	−1.8*	−2.13	−6.3*	−4.5*	6.86
	40	0.92	−1.2*	−0.75	−5.2*	−3.1*	6.32
	50	1.70	−0.5*	0.54	−4.4*	−2.1*	5.87
350	10	−2.63	−4.38	−5.90	−8.38	−8.08	8.33
	20	−1.53	−3.20	−4.23	−7.18	−6.11	7.35
	30	−0.65	−2.4*	−2.81	−6.3*	−4.7*	6.68
	40	0.13	−1.7*	−1.52	−5.3*	−3.4*	6.15
	50	0.86	−1.1*	−0.31	−4.6*	−2.4*	5.72
	60	1.56	−0.54	0.84	−3.8*	−1.5*	5.35
400	10	−3.28	−4.81	−6.41	−8.46	−8.52	8.18
	20	−2.20	−3.60	−4.80	−7.26	−6.51	7.20
	30	−1.36	−2.8*	−3.45	−6.3*	−4.9*	6.54
	40	−0.62	−2.3*	−2.23	−5.5*	−3.7*	6.02
	50	0.07	−1.6*	−1.09	−4.7*	−2.75*	5.60
	60	0.73	−1.02	−0.02	−4.0*	−2.0*	5.24

log $K_{CaHCO_3^+}$: $CaHCO_3^+ = Ca^{2+} + HCO_3^-$
log $K_{CaCO_3^0}$: $CaCO_3^0 = Ca^{2+} + CO_3^{2-}$
log K_{CO_2} : $CO_2^0 + H_2O = HCO_3^- + H^+$
log $K_{HCO_3^-}$: $HCO_3^- = H^+ + CO_3^{2-}$
log $K_{Arag.}$: $CaCO_3^{Arag} = Ca^{2+} + CO_3^{2-}$
log K_{OH^-} : $H^+ + OH^- = H_2O$

The results of the regression calculations are represented by the solid curves in Fig. 7 and the equilibrium constants given in Table 3. It can be seen that the solid curves closely fit the experimental Raman speciation data at pressures of 30 kbar and greater within the uncertainties of most of the data points. A direct test of the speciation/solubility model would involve an additional set of solubility measurements. In the present study, a semi-quantitative estimate of the solubilities has been obtained from the observed changes in size and shape of the aragonite crystals in the diamond anvil cell (e.g. Fig. 3). It can be seen in Fig. 8 that rather close agreement exists between these solubilities and the theoretical model solubilities, which strongly supports the overall validity of our speciation model.

Other results from the speciation/solubility calculations are also shown in Fig. 8. These include the predicted pH values and the full aqueous speciation of C-bearing species. It can be seen that the predicted solubilities in terms of $\log(m_{Ca^{2+}})$ reach values as high as −0.37 at 60 kbar and 350 °C, i.e. 422 mmolal. The pH is predicted to decrease from about 6.0 to 5.0 between 10 and 50 kbar, which is strongly alkaline compared to neutral pH at these conditions (Fig. 8D–F). Finally, the aqueous C-speciation, as expected, shows a predominance of HCO_3^- species below about 40 kbar, and a predominance of the CO_3^{2-} ion at higher pressures. Under most conditions it can be seen in Fig. 8G–I that the neutral species $CO_{2,aq}$ is a minor species, and even at 400 °C is predicted to decrease strongly relative to the HCO_3^- and CO_3^{2-} ions as a function of increasing pressure.

4.2.2. Implications for C-speciation in deep crustal and upper mantle supercritical aqueous fluids

The results described above represent a first step towards understanding and being able to predict the speciation of oxidized C in supercritical aqueous fluids at depths in the Earth greater than previously possible. The complex nature of the speciation inferred in the present study certainly suggests that the assumption that supercritical fluids in the Earth only contain dissolved oxidized C as the species $CO_{2,aq}$ is likely to be misleading. Our results indicate that more experimental data for the solubilities and speciation of fluids in equilibrium with other carbonate minerals are needed particularly at elevated pressures, for example for magnesite, dolomite and siderite.

It should be emphasized in this regard that the model results shown in Fig. 8 are specific to the pressures, temperatures and equilibrium with aragonite. In the deep crust and upper mantle, and particularly in and above subduction zones, such a wide range of pressures and temperatures exists that a huge range of speciation seems likely. This in turn will require much more experimental data and theoretical modeling to unravel.

Perhaps even more importantly, the speciation of dissolved oxidized C at any given pressure and temperature will depend very strongly on the environment with which the aqueous fluid is in contact. For example, the fluid pH values defined in the present study can only be expected to apply to fluids in equilibrium with aragonite. Different pH values can be expected to result from equilibration with different carbonate minerals (e.g. magnesite). Large differences can also be expected in silicate rock environments

where the activity ratios of cations to the H^+ ion, e.g. $a_{Ca^{2+}}/(a_{H^+})_2$, are controlled by silicate mineral assemblages in equilibrium with the supercritical fluid.

4.2.3. Implications for aqueous species equations of state

The revised values for log $K_{Arag.}$ and log $K_{HCO_3^-}$ in Table 3 are more than several log units smaller at high pressures than those predicted using the original equation of state parameters for the CO_3^{2-} and HCO_3^- ions from Shock and Helgeson (1988). These discrepancies are shown at 300–400 °C in the graphs in Fig. 9A and B. For example, at 50 kbar the discrepancies are about five log units. Interestingly, it is approximately the same discrepancy for the two equilibria at any given pressure and temperature, which strongly supports the assumption that it is primarily the properties of the carbonate ion that are to blame. It will be shown below that the discrepancy can be accounted for by revision of the equation of state parameters primarily for the carbonate ion.

In the HKF equation for the standard partial molal Gibbs free energy of an aqueous species (Appendix Eq. (A3)), changes with pressure at a given temperature depend on the four volume coefficients a_1, a_2, a_3, a_4, as well as the Born solvation coefficient ω for that species. However, when P is large (e.g. >20 kbar), the calculated changes of G with pressure are dominated by the coefficient a_1. This effect arises because changes in G are proportional to $a_1(P - Pr)$. Indeed, preliminary calculations confirmed that changing the value of a_1 for the carbonate ion could completely account for the discrepancies shown in Fig. 9 and Table 3 for both equilibria at a single temperature.

The solid curves shown in Fig. 10A–D were calculated with an a_1 value for the carbonate ion of 0.58 cal mole^{-1} bar^{-1} (c.f. 0.29 cal mole^{-1} bar^{-1} in Shock and Helgeson, 1988, Appendix). This revised value was obtained by simultaneously getting a best fit of the log $K_{Arag.}$ values in Fig. 10 and keeping as close a consistency as possible with experimental values of the standard partial molal volume

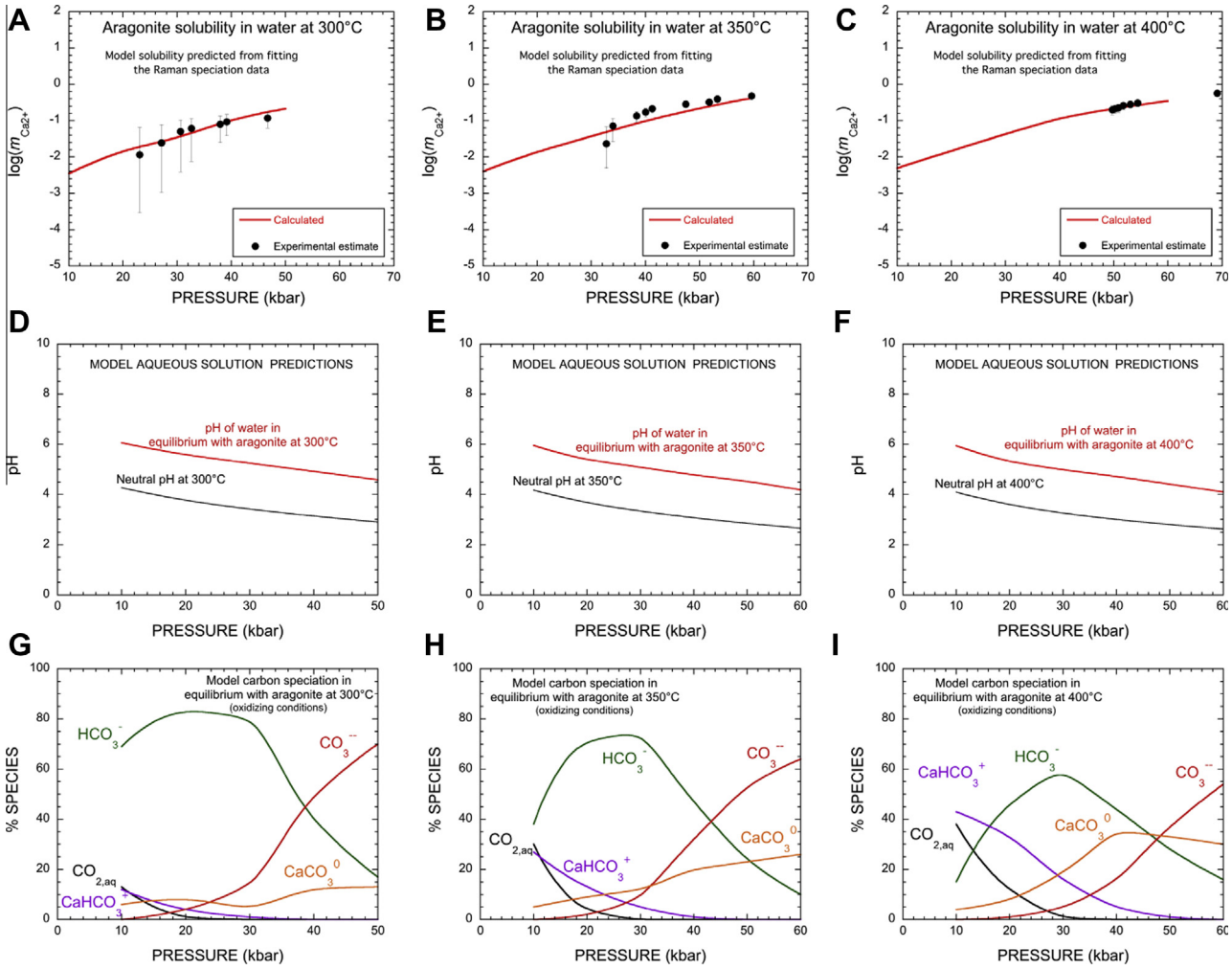

Fig. 8. Theoretical predictions of the aqueous speciation model constrained in Fig. 7. Aragonite solubility in water at 300 (A), 350 (B) and 400 °C (C). Predicted solubilities of aragonite compare favorably with those estimated by the shape change technique (see text). Model predictions of pH at 300 (D), 350 (E) and 400 °C (F). Model carbon speciation in equilibrium with aragonite at 300 (G), 350 (H) and 400 °C (I) (oxidizing conditions).

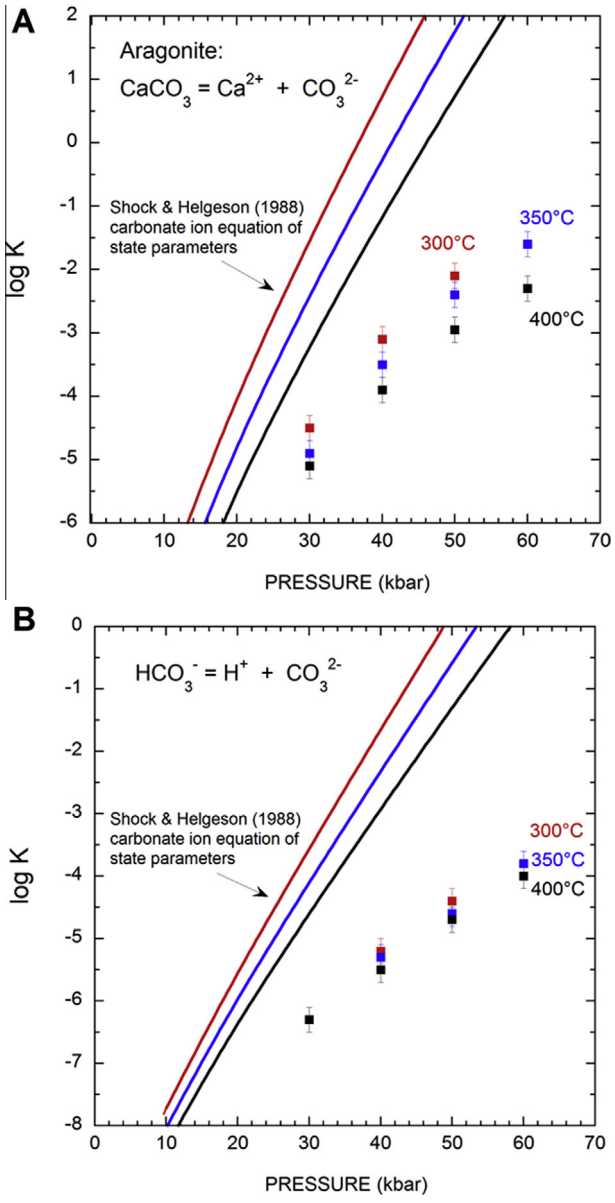

Fig. 9. The dashed curves represent predictions of the equilibrium constants using the HKF equations of state and the original equation of state parameters for HCO_3^- and CO_3^{2-} from Shock and Helgeson (1988) and Shock et al. (1989).

($V^0 = -5.0\ cm^3\ mole^{-1}$) of the carbonate ion at 25 °C and 1 bar and with the other linear correlations from Shock and Helgeson (1988) described in the Appendix. The latter have been widely used to estimate equation of state coefficients when the temperature dependence of the volume and compressibility are not available.

The final revised values of the volume coefficients for the carbonate ion given in Table 3 are thus consistent with the high pressure log K values derived from the Raman data and also with low pressure and temperature equilibria. The retrieval of the coefficient a_1 for the carbonate ion from the high pressure log $K_{Arag.}$ values enables an excellent description of the entire pressure range used experimentally (Fig. 10A). It can also be seen in Fig. 10C that when the revised carbonate ion equation of state parameters were used to predict values of log $K_{HCO_3^-}$, the agreement with the experimentally derived values is excellent. This agreement strongly supports the assumption that the main ion which needed revision was the carbonate ion. This is understandable because the original a_1 value for the carbonate ion given in Shock and Helgeson (1988) was derived indirectly from the combination of a correlation of $\sigma = a_1 + a_2/(P + \psi)$ with ΔV_n^0 (Appendix Eq. (A11)) and the predicted value of a_2 from the compressibility. Under these circumstances, the scatter on the correlation of σ with ΔV_n is too great to yield sufficiently accurate values of a_1 for calculations at the very high pressures of the present study.

Final calculated values of the equilibrium constants $K_{Arag.}$ and $K_{HCO_3^-}$ are also shown as a function of temperature in Fig. 10B and D. It can be seen in these figures that the results of the present study are consistent with experimentally derived equilibrium constants from ambient pressure and temperature up to high pressures and temperatures. The fact that the thermodynamic properties of the species used in the calculations are closely consistent with such a wide range of experimental values provides strong support for the internal consistency and the validity of the HKF approach over an enormous range of pressures and temperatures.

The new value of a_1 for the carbonate ion also has important implications for the general predictive model for aqueous species developed in Shock and Helgeson (1988). When experimental data for aqueous species as a function of temperature and pressure are lacking, the predictive model uses empirical linear correlations to estimate values of the equation of state coefficients from values of the standard partial molal volumes and heat capacities referring to 25 °C and 1 bar (see Appendix Eqs. (A4–A13)). For the parameter a_1, the crucial correlation originally developed in Shock and Helgeson (1988) is reproduced in Fig. 11A. It can be seen in the figure that this original correlation of a_1 with ΔV_n (Shock and Helgeson, 1988) contained a mixture of monovalent and divalent ions. The five ions originally presented had values of a_1 which were all derived from a combined regression of the temperature dependencies of experimentally derived volumes and compressibilities.

The revised correlation for predicting values of a_1 for divalent ions is shown in Fig. 11B (Appendix Eq. (A14)). This correlation strongly suggests that the Mg^{2+}, CO_3^{2-} and SO_4^{2-} ions form a separate correlation from the monovalent species. In turn, this will provide a basis for revisions to the estimated equation of state coefficients for all other divalent ions, as well as revised predictions for trivalent ions. In the case of neutral species, such as $CO_{2,aq}$ used in the present theoretical model, an additional separate predictive equation for a_1 values has been developed in a companion study (Sverjensky et al., 2014; see also Appendix Eq. (A15)). The development of this equation is based on well-constrained values for a_1 and $\Delta \bar{V}_n^0$ for glycine, methanol, ethanol, acetic acid, propanol and propanoic acid for which volumes and compressibilities were available (Plyasunov and Shock, 2001), and is supported by the regression of high pressure solubility and speciation data for neutral

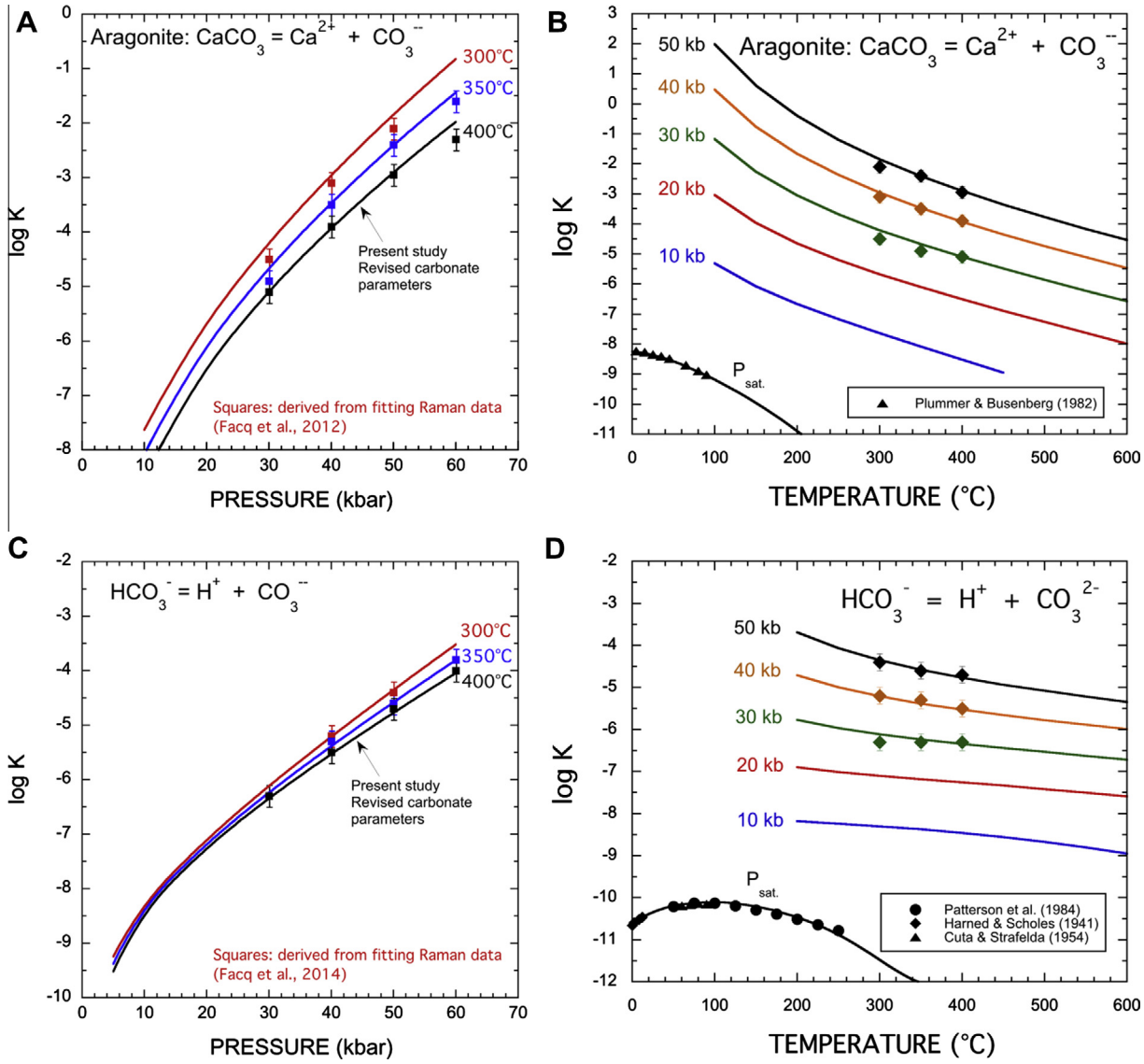

Fig. 10. Solid squares and diamonds at elevated pressures represent values of the logarithms of the equilibrium constants log $K_{\text{Arag.}}$ and log $K_{HCO_3^-}$ retrieved from fitting the Raman speciation data (Table 3): (A and B) The solid curves for log $K_{\text{Arag.}}$ represent a fit to the data using revised values of the equation of state parameters for the carbonate ion and other equation of state coefficients derived from experimental data and correlations (see text). (C and D) The solid curves for log $K_{HCO_3^-}$ represent a prediction using the revised values of the equation of state coefficients for the carbonate and bicarbonate ions.

aqueous species such as SiO_2^0 and $Si_2O_4^0$ (Sverjensky et al., 2014).

Overall, the experimental Raman speciation results and the thermodynamic model of carbonate solubility and aqueous speciation developed in the present study provide a strong basis for the application of the HKF aqueous equations of state to pressures of about 60 kbar. Together with the revised predictive correlations for the equation of state parameter a_1, the HKF equations and newly predicted equation of state parameters constitute a fully predictive model that can be applied to help interpret experimental results at elevated pressures and temperatures, as well as shedding new light on the role of water as a supercritical fluid in the Earth's deep crust and upper mantle.

5. CONCLUSIONS

We have carried out an integrated experimental and theoretical study of the carbonate speciation and aragonite solubility in water at 300–400 °C and pressures extending up to 70 kbar. The aqueous carbonate speciation was studied using *in situ* Raman spectroscopy in the diamond anvil cell. Approximate estimates of the solubility were obtained from observed changes in the size of the aragonite crystal in the cell. The experimental results were used to constrain the revised HKF equations of state for the carbonate and bicarbonate equilibria based on estimates of the dissociation constants of water, CO_2^0, and $CaHCO_3^+$. The results of our study are as follows:

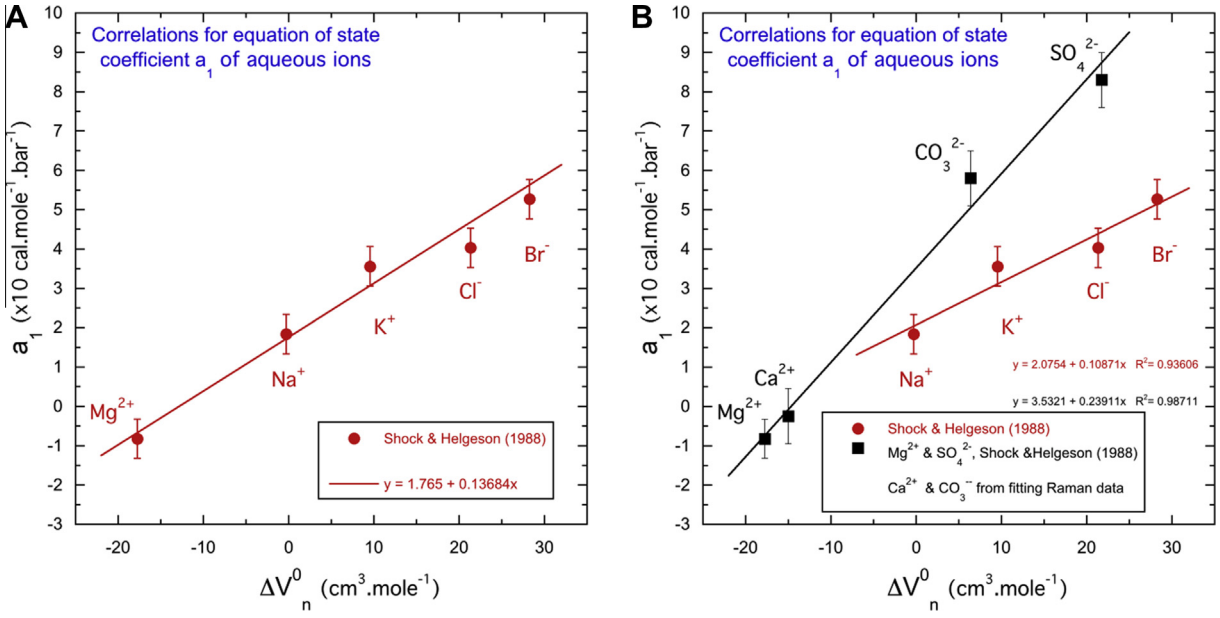

Fig. 11. Symbols represent values of the equation of state parameter a_1 for the ions shown: (A) Original linear correlation from Shock and Helgeson (1988) in which it was assumed that divalent and monovalent ions followed the same correlation line; (B) Revised correlations based on the present study in which divalent and monovalent ions define different correlation lines (see text).

(1) The experimental results demonstrate a systematic change in the proportions of HCO_3^- and CO_3^{2-} with increasing pressure. At all temperatures investigated, HCO_3^- species predominate over CO_3^{2-} species at pressures below about 40 kbar, whereas CO_3^{2-} species predominate above 40 kbar.

(2) The theoretical results indicate the broad applicability of the HKF equations of state for aqueous species at pressures far above those traditionally considered (e.g. 5.0 kbar). As a result of this application to the Raman constraints, the equation of state characterization of aqueous divalent ions has been revised relative to the original predictive algorithm developed by Shock and Helgeson (1988). Reactions involving other divalent ions can now be predicted at very high pressures for comparison with experimental data.

(3) The combined experimental and theoretical results indicate that it is likely that both HCO_3^- and the $CaHCO_3^+$ complex contribute to the total HCO_3^- species detected by Raman spectroscopy at the lower pressures, whereas both CO_3^{2-} and the $CaCO_3^0$ complex contribute at the higher pressures.

(4) These results contrast with the previously hypothesized predominance of $CO_{2,aq}$ in aqueous fluids at high temperatures and lower pressures. Our results suggest that ion-pairing in deep crustal and mantle aqueous fluids may occur during the dissolution of carbonate minerals at high pressure. Ultimately, the speciation of oxidized carbon in deep Earth fluids will, however, depend on a complex interplay of pressure, temperature, and activity ratios imposed by the silicate and/or carbonate environment in the Earth.

ACKNOWLEDGMENTS

The authors wish to acknowledge the support and collaboration of the 'Reservoirs and Fluxes' and 'Extreme Physics and Chemistry' communities of the Deep Carbon Observatory. The Raman facility at the École Normale Supérieure de Lyon is supported by the Institut National des Sciences de l'Univers (INSU). Additional support was provided by Grants DOE DE-FG-02-96ER-14616 and NSF EAR 1023865 to Sverjensky. We thank Associate Editor R. Dasgupta and three anonymous reviewers for their helpful comments on the manuscript. We gratefully acknowledge the help and support of the Johns Hopkins University, the Geophysical Laboratory of the Carnegie Institution of Washington, and the Université Claude Bernard Lyon 1.

APPENDIX A. SUPPLEMENTARY DATA

Supplementary data associated with this article can be found, in the online version, at http://dx.doi.org/10.1016/j.gca.2014.01.030.

REFERENCES

Bandura A. V. and Lvov S. N. (2006) The ionization constant of water over wide ranges of temperature and density. *J. Phys. Chem. Ref. Data* **35**, 15–30.

Berman R. G. (1988) Internally-consistent thermodynamic data for minerals in the system Na_2O-K_2O-CaO-MgO-FeO-Fe_2O_3-Al_2O_3-SiO_2-TiO_2-H_2O-CO_2. *J. Petrol.* **29**, 445–522.

Berman R. G. and Aranovich L. Y. (1996) Optimized standard state and solution properties of minerals. *Contrib. Mineral. Petrol.* **126**, 1–24.

Berner R. A. (1999) A new look at the long-term carbon cycle. *GSA Today* **9**, 1–6.

Caciagli N. C. and Manning C. E. (2003) The solubility of calcite in water at 6–16 kbar and 500–800 °C. *Contrib. Mineral. Petrol.* **146**, 275–285.

Chervin J. C., Canny B., Besson J. M. and Pruzan Ph. (1995) A diamond anvil cell for IR microspectroscopy. *Rev. Sci. Instrum.* **66**, 2595–2598.

Colthup N. B., Daly L. H. and Wiberley S. E. (1975) *Introduction to Infrared and Raman spectroscopy*. Academic Press, New York, p. 523.

Dasgupta R. (2013) Ingassing, storage, and outgassing of terrestrial carbon through geologic time. *Rev. Mineral. Geochem.* **75**, 183–229.

Dasgupta R. and Hirschmann M. M. (2010) The deep carbon cycle and melting in Earth's interior. *Earth Planet. Sci. Lett.* **298**, 1–13.

Dasgupta R., Hirschmann M. M. and Dellas N. (2005) The effect of bulk composition on the solidus of carbonated eclogite from partial melting experiments at 3 GPa. *Contrib. Mineral. Petrol.* **149**, 288–305.

Datchi F., Loubeyre P. and LeToullec R. (2000) Extended and accurate determination of the melting curves of argon, helium, ice (H_2O), and hydrogen (H_2). *Phys. Rev. B* **61**, 6535–6546.

Davis A. R. and Oliver B. G. (1972) A vibrational-spectroscopic study of the species present in the CO_2–H_2O system. *J. Solution Chem.* **1**, 329–339.

Dolejš D. (2013) Thermodynamics of aqueous species at high temperatures and pressures: Equations of state and transport theory. *Rev. Mineral. Geochem.* **76**, 35–79.

Dolejš D. and Manning C. E. (2010) Thermodynamic model for mineral solubility in aqueous fluids: theory, calibration and application to model fluid-flow systems. *Geofluids* **10**, 20–40.

Dove M. T. and Powell B. M. (1989) Neutron diffraction study of the tricritical orientational order/disorder phase transition in calcite at 1260 K. *Phys. Chem. Minerl.* **16**, 503–507.

Dubessy J., Moissette A., Bakker R. J., Frantz J. D. and Zhang Y.-G. (1999) High-temperature Raman spectroscopic study of H_2O–CO_2–CH_4 mixtures in synthetic fluid inclusions: first insights on molecular interactions and analytical implications. *Eur. J. Mineral.* **11**, 23–32.

Evans K. A. (2012) The redox budget of subduction zones. *Earth Sci. Rev.* **113**, 11–32.

Fein J. B. and Walther J. V. (1987) Calcite solubility in supercritical CO_2–H_2O fluids. *Geochim. Cosmochim. Acta* **51**, 1665–1673.

Fein J. B. and Walther J. V. (1989) Calcite solubility and speciation is supercritical NaCl–HCl aqueous fluids. *Contrib. Mineral. Petrol.* **103**, 317–324.

Fiquet G., Guyot F. and Itié J.-P. (1994) High-pressure X-ray diffraction study of carbonates: $MgCO_3$, $CaMg(CO_3)_2$, and $CaCO_3$. *Am. Mineral.* **79**, 15–23.

Fong M. Y. and Nicol M. (1971) Raman spectrum of calcium carbonate at high pressures. *J. Chem. Phys.* **54**, 579–585.

Franck E. U., Rosenzweig S. and Christoforakos M. (1990) Calculation of the dielectric constant of water to 1000-degrees-c and very high-pressures. *Ber. Bunsenges. Chem. Phys.* **94**, 199–203.

Frantz J. (1998) Raman spectra of potassium carbonate and bicarbonate aqueous fluids at elevated temperatures and pressures: comparison with theoretical simulations. *Chem. Geol.* **152**, 211–225.

Frantz J. D., Dubessy J. and Mysen B. O. (1994) Ion-pairing in aqueous $MgSO_4$ solutions along an isochore to 500 °C and 11 kbar using Raman spectroscopy in conjunction with the diamond-anvil cell. *Chem. Geol.* **116**, 181–188.

Frezzotti M. L., Selverstone J., Sharp Z. D. and Compagnoni R. (2011) Carbonate dissolution during subduction revealed by diamond-bearing rocks from the Alps. *Nat. Geosci.* **4**, 703–706.

Gillet P., Malezieux J.-M. and Dhamelincourt M.-C. (1988) MicroRaman multichannel spectroscopy up to 2.5 GPa using a sapphire-anvil cell: experimental set-up and some applications. *Bull. Mineral.* **111**, 1–15.

Gillet P., Biellmann C., Reynard B. and McMillan P. (1993) Raman spectroscopic studies of carbonates Part I: High-pressure and high-temperature behaviour of calcite, magnesite, dolomite and aragonite. *Phys. Chem. Mineral.* **20**, 1–18.

Heger K., Uematsu M. and Franck E. U. (1980) The static dielectric constant of water at high pressures and temperatures to 500 MPa and 550 °C. *Ber. Bunsenges. Phys. Chem.* **84**, 758–762.

Helgeson H. C. and Kirkham D. H. (1976) Theoretical prediction of the thermodynamic properties of aqueous electrolytes at high pressures and temperatures. III. Equation of state for aqueous species at infinite dilution. *Am. J. Sci.* **276**, 97–240.

Helgeson H. C., Kirkham D. H. and Flowers G. C. (1981) Theoretical prediction of the thermodynamic behavior of aqueous electrolytes at high pressures and temperatures. IV. Calculation of activity coefficients, osmotic coefficients, and apparent molal and standard and relative partial molal properties to 5 kb and 600 °C. *Am. J. Sci.* **281**, 1241–1516.

Hnedkovsky L. and Wood R. H. (1997) Apparent molar heat capacities of aqueous solutions of CH_4, CO_2, H_2S, and NH_3 at temperatures from 304 K to 704 K at a pressure of 28 MPa. *J. Chem. Thermodyn.* **29**, 731–747.

Johnson J. W., Oelkers E. H. and Helgeson H. C. (1992) SUPCRT92: a software package for calculating the standard molal thermodynamic properties of minerals, gases, aqueous species, and reactions from 1 to 5000 bars and 0 to 1000 °C. *Comput. Geosci.* **18**, 899–947.

Kerrick D. M. and Connolly J. A. D. (1998) Subduction of ophicarbonates and recycling of CO_2 and H_2O. *Geology* **26**, 375–378.

Kerrick D. M. and Connolly J. A. D. (2001) Metamorphic devolatilization of subducted oceanic metabasalts: implications for seismicity, arc magmatism and volatile recycling. *Earth Planet. Sci. Lett.* **189**, 19–29.

Lin S.-H. and Huang W.-L. (2004) Polycrystalline calcite to aragonite transformation kinetics: experiments in synthetic systems. *Contrib. Mineral. Petrol.* **147**, 604–614.

Liu L.-G. and Mernagh T. P. (1990) Phase transitions and Raman spectra of calcite at high pressures and room temperature. *Am. Mineral.* **75**, 801–806.

Manning C. E., Shock E. L. and Sverjensky D. A. (2013) The chemistry of carbon in aqueous fluids at crustal and upper-mantle conditions: experimental and theoretical constraints. Ch. 5. In *Carbon in Earth* (eds. R. M. Hazen, J. A. Baross and A. P. Jones). Mineralogical Society of America.

Marshall W. L. and Franck E. U. (1981) Ion product of water substance, 0 °C–1000 °C, 1–10,000 bars – new international formulation and its background. *J. Phys. Chem. Ref. Data* **10**, 295–304.

Martinez I., Zhang J. and Reeder R. J. (1996) In-situ X-ray diffraction of aragonite and dolomite at high pressure and high temperature: evidence for dolomite breakdown to aragonite and magnesite. *Am. Minerl.* **81**, 611–624.

Martinez I., Sanchez-Valle C., Daniel I. and Reynard B. (2004) High-pressure and high-temperature Raman spectroscopy of carbonate ions in aqueous solution. *Chem. Geol.* **207**, 47–58.

Matas J., Gillet P., Ricard Y. and Martinez I. (2000) Thermodynamic properties of carbonates at high pressures from vibrational modelling. *Eur. J. Mineral.* **12**, 703–720.

Mirwald P. W. (1976) A differential thermal analysis study of the high-temperature polymorphism of calcite at high pressure. *Contrib. Mineral. Petrol.* **59**, 33–40.

Mirwald P. W. (1979) The electrical conductivity of calcite between 300 and 1200 °C at a CO_2 pressure of 40 bars. *Phys. Chem. Minerl.* **4**, 291–297.

Morse J. W. and Mackenzie F. T. (1990) *Geochemistry of Sedimentary Carbonates*. Elsevier, Amsterdam, p. 707.

Newton R. and Manning C. (2002) Experimental determination of calcite solubility in H_2O–NaCl solutions at deep-crust/upper mantle pressures and temperatures: implications for metasomatic processes in shear zones. *Am. Mineral.* **87**, 1401–1409.

Oliver B. G. and Davis A. R. (1973) Vibrational spectroscopic studies of aqueous alkali-metal bicarbonate and carbonate solutions. *Can. J. Chem.* **51**, 698–702.

Pan D., Spanu L., Harrison B., Sverjensky D. A. and Galli G. (2013) Dielectric properties of water under extreme conditions and transport of carbonates in the deep Earth. *Proc. Natl. Acad. Sci. U.S.A.* **110**, 6646–6650.

Plummer L. N. and Busenberg E. (1982) The solubilities of calcite, aragonite and vaterite in CO_2–H_2O solutions between 0 to 90 °C and an evaluation of the aqueous model for the system $CaCO_3$–CO_2–H_2O. *Geochim. Cosmochim. Acta* **46**, 1011–1040.

Plyasunov A. V. and Shock E. L. (2001) Correlation strategy for determining the parameters of the revised Helgeson–Kirkham–Flowers model for aqueous nonelectrolytes. *Geochim. Cosmochim. Acta* **65**, 3879–3900.

Redfern S. A. T., Salje E. and Navrotsky A. (1989) High-temperature enthalpy at the orientational order-disorder transition in calcite: implications for the calcite/aragonite phase equilibrium. *Contrib. Mineral. Petrol.* **101**, 479–484.

Sanchez-Valle C. (2013) Structure and thermodynamics of subduction zone fluids from spectroscopic studies. *Rev. Mineral. Geochem.* **76**, 265–309.

Sano Y. and Williams S. N. (1996) Fluxes of mantle and subducted carbon along convergent plate boundaries. *Geophys. Res. Lett.* **23**, 2749–2752.

Schmidt C. (2009) Raman spectroscopic study of a $H_2O + Na_2SO_4$ solution at 21–600 °C and 0.1 MPa to 1.1 GPa: Relative differential v_1–SO_4^{2-} Raman scattering cross sections and evidence of the liquid–liquid transition. *Geochim. Cosmochim. Acta* **73**, 425–437.

Shock E. L. and Helgeson H. C. (1988) Calculation of the thermodynamic and transport properties of aqueous species at high pressures and temperatures: Correlation algorithms for ionic aqueous species and equation of state predictions to 5 kb and 1000 °C. *Geochim. Cosmochim. Acta* **52**, 2009–2036.

Shock E. L. and Helgeson H. C. (1990) Calculation of the thermodynamic and transport properties of aqueous species at high pressures and temperatures: Standard partial molal properties of organic species. *Geochim. Cosmochim. Acta* **54**, 915–945.

Shock E. L. and Koretsky C. M. (1995) Metal–organic complexes in geochemical processes: Estimation of standard partial molal thermodynamic properties of aqueous complexes between metal cations and monovalent organic acid ligands at high pressures and temperatures. *Geochim. Cosmochim. Acta* **59**, 1497–1532.

Shock E. L., Helgeson H. C. and Sverjensky D. A. (1989) Calculation of the thermodynamic and transport properties of aqueous species at high pressures and temperatures: standard partial molal properties of inorganic neutral species. *Geochim. Cosmochim. Acta* **53**, 2157–2184.

Shock E. L., Sassani D. C., Willis M. and Sverjensky D. A. (1997) Inorganic species in geologic fluids: correlations among standard molal thermodynamic properties of aqueous cations, oxyanions, acid oxyanions, oxyacids and hydroxide complexes. *Geochim. Cosmochim. Acta* **61**, 907–950.

Stefansson A., Bénézeth P. and Schott J. (2013) Carbonic acid ionization and the stability of sodium bicarbonate and carbonate ion pairs to 200 °C: a potentiometric and spectrophotometric study. *Geochim. Cosmochim. Acta* **120**, 600–611.

Suito K., Namba J., Horikawa T., Taniguchi Y., Sakurai N., Kobayashi M., Onodera A., Shimomura O. and Kikegawa T. (2001) Phase relations of $CaCO_3$ at high pressure and high temperature. *Am. Mineral.* **86**, 997–1002.

Sverjensky D. A., Shock E. L. and Helgeson H. C. (1997) Prediction of the thermodynamic properties of aqueous metal complexes to 1000 °C and 5 kb. *Geochim. Cosmochim. Acta* **61**, 1359–1412.

Sverjensky D. A., Harrison B. and Azzolini D. (2014) Water in the deep Earth: The dielectric constant and the solubilities of quartz and corundum to 60 kb and 1,200 °C. *Geochimica et Cosmochimica Acta* **129**, 125–145.

Sweeton F. H., Mesmer R. E. and Baes, Jr., C. F. (1974) Acidity measurements at elevated temperatures. VII. Dissociation of water. *J. Solution. Chem.* **3**, 191–214.

Syracuse E. M., van Keken P. E. and Abers G. A. (2010) The global range of subduction zone thermal models. *Phys. Earth Planet. Inter.* **183**, 73–90.

Thomsen T. B. and Schmidt M. W. (2008) Melting of carbonaceous pelites at 2.5–5 GPa, silicate–carbonatitie liquid immiscibility, and potassium–carbon metasomatism of the mantle. *Earth Planet. Sci. Lett.* **267**, 17–31.

Tsuno K. and Dasgupta R. (2012) The effect of carbonates on near-solidus melting of pelite at 3 GPa: relative efficiency of H_2O and CO_2 subduction. *Earth Planet. Sci. Lett.* **319–320**, 185–196.

Walther, J. V. and Long, M. I. (1986) Experimental determination of calcite solubilities in supercritical H_2O. *Fifth International Symposium on Water–Rock Interaction*. pp. 609–611.

Wolery T. J. (1983) EQ3NR: a computer program for geochemical aqueous speciation-solubility calculations. *User's Guide and Documentation*. UCRL-53414. Lawrence Livermore Lab., Univ. Calif.

Yaxley G. M. and Green D. H. (1994) Experimental demonstration of refractory carbonate-bearing ecoglite and siliceous melt in the subduction regime. *Earth Planet. Sci. Lett.* **128**, 313–325.

Zhang Z. and Duan Z. (2005) Prediction of the PVT properties of water over wide range of temperatures and pressures from molecular dynamics simulation. *Phys. Earth Planet. In.* **149**, 335–354.

Associate editor: Rajdeep Dasgupta